UC Berkeley

UC Berkeley Previously Published Works

Title

Patterned Electrospinning: A Method of Generating Defined Fibrous Constructs Influencing Cell Adhesion and Retention

Permalink

https://escholarship.org/uc/item/8hn9m589

Journal

ACS Applied Bio Materials, 4(5)

ISSN

2576-6422

Authors

Palomares, Daniel
Ammann, Kaitlyn R
Perez, Javier J Saldana
et al.

Publication Date

2021-05-17

DOI

10.1021/acsabm.0c01311

Peer reviewed

eScholarship.org Powered by the California Digital Library
University of California

Author Manuscript

Author Manuscript

Author Manuscript

Author Manuscript

HHS Public Access

Author manuscript

ACS Appl Bio Mater. Author manuscript; available in PMC 2022 September 05.

Published in final edited form as:

ACS Appl Bio Mater. 2021 May 17; 4(5): 4084–4093. doi:10.1021/acsabm.0c01311.

Patterned Electrospinning: A Method of Generating Defined Fibrous Constructs Influencing Cell Adhesion and Retention

Daniel Palomares,
Department of Biomedical Engineering, University of Arizona, Tucson, Arizona 85721-0072, United States

Kaitlyn R. Ammann,
Department of Medicine and Sarver Heart Center, University of Arizona, Tucson, Arizona 85721-0072, United States

Javier J. Saldana Perez,
Department of Biomedical Engineering, University of Arizona, Tucson, Arizona 85721-0072, United States

Alexan Gomez,
Department of Biomedical Engineering, University of Arizona, Tucson, Arizona 85721-0072, United States

Adriana Barreda,
Department of Biomedical Engineering, University of Arizona, Tucson, Arizona 85721-0072, United States

Andrew Russell-Cheung,
Department of Biological & Biomedical Sciences, University of Arizona, Tucson, Arizona 85721-0001, United States

Adriana Martin,
Sarver Heart Center, University of Arizona, Tucson, Arizona 85721-0001, United States

Phat Le Tran,
Department of Bioengineering, University of California, Berkeley, California 94720, United States

Sahir Hossainy,
Sarver Heart Center, University of Arizona, Tucson, Arizona 85721-0001, United States

Rebecca C. Slepian,
Sarver Heart Center, University of Arizona, Tucson, Arizona 85721-0001, United States

Syed F.A. Hossainy,
Department of Bioengineering, University of California, Berkeley, California 94720, United States

Marvin J. Slepian

Corresponding Author: Marvin J. Slepian – Department of Biomedical Engineering, Department of Medicine, and Sarver Heart Center, University of Arizona, Tucson, Arizona 85721-0072, United States; slepian@email.arizona.edu.

Complete contact information is available at: https://pubs.acs.org/10.1021/acsabm.0c01311

The authors declare no competing financial interest.

Author Manuscript Author Manuscript Author Manuscript Author Manuscript

Department of Biomedical Engineering, Department of Medicine, and Sarver Heart Center, University of Arizona, Tucson, Arizona 85721-0072, United States

Abstract

A critical component of tissue engineering is the ability to functionally replace native tissue stroma. Electrospinning is a technique capable of forming fibrous constructs with a high surface area for increased cell–material interaction and enhanced biocompatibility. However, physical and biological properties of electrospun scaffolds are limited by design controllability on a macroscale. We developed a methodology for generating electrospun scaffolds with defined patterns and topographic features to influence physical properties and biological interactions. Five unique design electrospinning target collectors were fabricated to allow for generation of defined polymeric scaffold patterns including lines, sinusoids, squares, zigzags, and solid. Poly(lactic-*co*-glycolic) acid was electrospun under identical conditions utilizing these varied targets, and constructs generated were examined as to their physical configuration, mechanical and chemical properties, and their ability to foster vascular smooth muscle cell adhesion and retention at 24 h. Modifying collector designs led to significant differences in fiber target coverage ranging from 300 mm^2 for solid (100% of the target area) to 217.8 mm^2 for lines (72.6% of the target area). Measured fiber excess, residual open area, and contact angle (hydrophobicity) followed the same trend as fiber target coverage with respect to the collector pattern: lines > sinusoids > squares > zigzags > solid. Similarly, the line design allowed for the greatest cell adhesion and retention (258 ± 31 cells), whereas solid exhibited the lowest (150 ± 15 cells); $p < 0.05$. There was a strong direct correlation of cell adhesion to construct residual open area ($R^2 = 0.94$), normalized fiber excess ($R^2 = 0.99$), and fiber grammage ($R^2 = 0.72$), with an inverse relationship to fiber target coverage ($R^2 = 0.94$). Our results demonstrate the ability to utilize patterned collectors for modifying macroscopic and microscopic electrospun scaffold features, which directly impact cell adhesion and retention, offering translational utility for designing specific tissue constructs.

Graphical Abstract

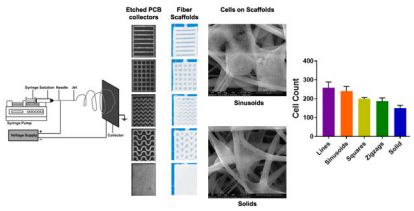

Keywords

electrospinning; patterned targets; scaffolds; PLGA; tissue engineering; tissue stroma; extracellular matrix; tissue architecture; cell adhesion; fiber grammage

INTRODUCTION

A fundamental goal of tissue engineering is repair, augmentation, or frank replacement of organs or organ components due to compromise occurring as a result of a disease or injury.[1,2] A vital component of tissue engineering is fabrication of functional scaffolds,

Author Manuscript Author Manuscript Author Manuscript Author Manuscript

or stroma, upon which organ-specific cells may populate, function, and thrive.[3–5] Native tissue stroma are typically complex three-dimensional porous structures with a wide range of interstices, pore sizes, complex layered arrangements, and other irregular topographies. The spectrum of stromal configurations relates to differing needs and optima for specific cell types and organ functions. Attempting to recapitulate these structures *in vitro* or *in vivo* has been difficult to date. A variety of approaches have been utilized to attempt this including growing cell monolayers with subsequent cell-based remodeling of the underlying matrix, degrading fabricated matrices to create pores, decellularizing/devitalizing organs *ex vivo* to generate residual basal matrices for repurposed use, cell aggregation techniques with admixed matrix elements, and a range of layered matrix fabrication techniques.[6–9] Each of these methodologies has been defined, often with significant limitations.[2,10,11] As such, new methods allowing for predictable pattern generation of stromal biomaterials, either native or synthetic, are needed. We address this issue here.

Electrospinning is a recognized methodology for the replication of tissue stroma and matrix composition, topography, and mechanical properties.[12–15] Electrospinning utilizes an applied electrical field to induce an electrical potential between an extruded polymer solution and a grounded collector.[12,13,16,17] In practice, electromagnetic force creates a fine jet of polymer solution, allowing a solvent to rapidly evaporate during extrusion, leaving behind polymeric fibers on the electrically grounded collector.[12,13] Most of the steps in the electrospinning process are modifiable to create fibrous constructs of designated dimensions, within a range, for a desired application. Previous work has focused on modulating both the material and collector properties to further improve the biocompatibility of electrospun substrates.[18–20] Electrospinning can be performed with either synthetic or biologic materials. Our group has previously developed composite core–shell electrospun nanofibers containing polyvinyl alcohol and gelatin to modulate fiber mechanical properties,[21] bioactivity and biocompatibility,[22] and hemocompatibility.[23] Yet, despite the potential of electrospinning, it remains limited by the random nature of the geometry and topography of constructs typically generated.

The physical and mechanical properties of substrates have been identified as important factors influencing cell growth and proliferation, beyond those dictated by the biochemical environment.[24,25] Electrospun substrates mimic extracellular matrix components with a characteristic high surface area-to-volume ratio and porosity of the underlying construct. Multiscale porosity is particularly desirable for an electrospun implant utilized for tissue regeneration. Cellular infiltration is favored by a porous matrix with large pores, while cellular adhesion, proliferation, and differentiation are typically dependent on a smaller fiber diameter and a high packing density.[25–29] Several methods have been described to achieve multiscale porosity.[30–36] In a typical electrospinning system, the grounded collector is an anchored, flat conductive metal surface, generating a solid fibrous sheet of an electrospun material.[12,13] Prior work has examined more complex approaches including rotating cylinders, liquid collectors that spindle fibers, and related methodologies in efforts to control fiber properties and configuration.[12,20,28,37,38] However, a simple pattern modification to a flat metal collector may aid in modulating fiber distribution at the 2D collector interface.

Author Manuscript Author Manuscript Author Manuscript Author Manuscript

In this study, we address the issue of generating defined electrospun configurations through modification of the shape of a flat metal collector within the electrospinning system. We hypothesized that changes in the metal collector target pattern will correspond directly to defined fiber configuration, patterns, and mechanical properties, all ultimately influencing vascular cell adhesion and retention. As a first step, we created five distinct patterns of 2D plate collectors to focus and target polymer jets of poly(lactic-*co*-glycolic) acid (PLGA) and examined the efficacy of this approach in constructing fibrous scaffolds of varying topographies and fiber distributions. We then examined the effect of fiber pattern configuration on construct mechanical and chemical properties. Finally, we examined the impact of fiber configuration and corresponding physical properties on vascular cell adhesion and retention.

EXPERIMENTAL METHODS

Patterned Collector Fabrication.

Five differing patterns were created for collectors: lines, squares, zigzags, sinusoids, and solid. The patterned collectors (3 × 1 cm each) were designed using a Copper Connection PCB editor (ExpressPCB, LLC). Designs were laser-printed onto Press-N-Peel blue transfer sheets (Techniks, Inc., Indianapolis, IN, USA) and heat-transferred to a clean, copper-clad circuit board laminate. The copper boards were submerged in an etching solution (2:1 mixture of 0.9 M H_2O_2/12 M HCl) for 40 min. Etched boards were then washed with acetone to remove the transfer sheet material, revealing copper designs as copper traces. Individual patterns are shown in Figure 1.

Polymer Scaffold Fabrication.

PLGA (95:5) solution was prepared with dichloromethane (DCM) as a solvent at 7.5% concentration (w/v) and vortexed for 45 min at room temperature. The resultant homogeneous solution was loaded within a horizontal syringe pump (New Era Pump Systems, Inc., Farmingdale, NY, USA). An extruding gauge needle (23 G) was connected to the cathode of a direct current power supply (12 kV), while the copper collector was grounded, creating an electrical potential. With current flowing, the PLGA solution was extruded at a rate of 2.5 mL/h jetted toward copper collector targets positioned at a distance of 15 cm (Figure 1).

A nonfibrous, i.e., continuous, PLGA sample was fabricated for reference by spin coating the PLGA solution at 500 rpm for 10 s using a spin coater (model PWM32, Headway Research, Inc., Garland, Texas, USA). Spin-coated continuous samples were used as a control for comparison to electrospun fibrous PLGA scaffolds for all studies performed.

Scaffold Physical Characterization.

The mass of fiber scaffolds was determined using an analytical balance (Mettler AE 100, Mettler Toledo, Columbus, OH, USA). The fiber diameter was determined via measurements from scanning electron microscopy (SEM) images obtained using a Hitachi-S4800 field emission SEM (Chiyoda, Tokyo, Japan; 500× magnification). Scaffold images

Author Manuscript Author Manuscript Author Manuscript Author Manuscript

were analyzed using ImageJ software (NIH Bethesda, MD) to determine the fiber diameter. The scale bar on each SEM image is presented as a dimensional control.

High-resolution images of each collector and PLGA scaffold were taken with a Nikon D7100 DSLR camera (Nikon, Inc., Melville, NY, USA) in a controlled lighting environment. Resultant images were converted to binary and analyzed in Adobe Photoshop CS5 Extended (Version 12.1, Adobe Systems, Incorporated, San Jose, CA, USA) to determine the pixel count of exposed copper traces, or PLGA fibers, for each design studied. A predetermined pixel/area ratio was utilized to convert the pixel count to mm^2.

To determine the surface area of the exposed copper target (copper traces) and the adherent polymer scaffold construct, as a % of the total target area (i.e., copper trace conductive area + nonconductive insulated area), the following values were calculated

$$\text{copper trace area } (\%) = (\text{ copper trace area } \div \text{ total area }) \times 100 \tag{1}$$

$$\text{fiber target coverage } (\%) = (\text{ fiber (scaffold) area total area }) \times 100 \tag{2}$$

where the copper trace area and fiber (scaffold) area were calculated from image pixel counts and converted to mm^2 and the total area is equal to a 3 × 1 cm scaffold area (300 mm^2) for all patterned designs.

The residual open area (%), a parameter allowing quantitation of macroscopic porosity of the fiber constructs generated, was calculated as

$$\text{residual open area } (\%) = 100 - \text{ fiber target coverage} \tag{3}$$

where figure target coverage is calculated from eq 2.

To investigate the efficacy of each pattern as a target and the accuracy of fiber deposition, i.e., how much coverage was achieved (full, less, or excessive), fiber excess was determined as the total area of PLGA fiber adhesion, which exceeded the bounds of the copper trace patterned area and was calculated as follows

$$\text{fiber excess } = \text{ fiber (scaffold) area } - \text{ copper trace area} \tag{4}$$

where the fiber (scaffold) area and copper trace area were calculated from image pixel counts and converted to mm^2 as previously mentioned in eq 1. While fiber excess is a characteristic parameter of the patterned collectors, in order to compare this parameter across differing designs, it was normalized as follows

$$\begin{aligned}&\text{normalized fiber excess } (\%)\\ &= (\text{ fiber excess } \div \text{ copper trace area }) \times 100\end{aligned} \tag{5}$$

where fiber excess is calculated from eq 4.

Author Manuscript Author Manuscript Author Manuscript Author Manuscript

We also calculated grammage, a common variable utilized to determine densities of porous fibrous constructs (e.g., paper). Grammage is the area density and was calculated for the constructs as fiber grammage (μg/mm^2) as follows

$$\text{fiber grammage} = \text{fiber scaffold mass} \div \text{fiber (scaffold) area} \quad (6)$$

where fiber scaffold mass was measured by utilizing an analytical balance, and the fiber (scaffold) area was measured as described in eq 1.

Scaffold Mechanical Characterization.

Mechanical characterization of scaffolds was determined using a Pyris Diamond dynamic mechanical analyzer (DMA) (PerkinElmer, Waltham, MA, USA). Uniaxial tensile analysis was performed on scaffolds while stretched at 50 μm/min to the point of failure. The elastic modulus and tensile strength were extrapolated from the stress versus strain data of each scaffold. Tensile strength was identified as the highest stress measured from the polymer construct during strain. All samples were strained to the point of failure. The elastic modulus was calculated according to eq 7, where F is the force exerted on the polymer sample, A is the sample cross-sectional area, L_0 is the initial sample length, and ΔL is the change in sample length after straining

$$E = \text{stress / strain} = (F/A)/(\Delta L/L_0) \quad (7)$$

Attenuated Total Reflectance-Fourier Transform Infrared (ATR-FTIR) Spectroscopy.

The chemical compositions of the electrospun PLGA fibers of each design were determined via attenuated total reflectance-Fourier transform infrared (ATR-FTIR) spectroscopy utilizing a Nicolet Avatar 360 FTIR spectrometer (Varian, Inc., CA) equipped with a deuterated triglycine sulfate (DTGS) detector and Harrick MNP-Pro (Pleasantville, NY, USA) and attenuated total reflectance (ATR). Similar spectra were obtained of raw (preprocessing) PLGA and of spin-coated PLGA as controls. Each spectrum was collected for 32 scans at a spectral resolution 2 cm^{-1} over a wavenumber range of 4000–400 cm^{-1}. A background spectrum was carried out under the same experimental conditions and was subtracted from each sample spectrum. Spectral data were acquired with EZ-OMnic software.

Contact Angle Determination.

Static sessile drop angle of deionized water (DIW) on the surface of fiber scaffolds was measured using an Optical System Cam 100 optical contact angle meter (DataPhysics Instruments USA Corp., 4424 Taggart Creek Road, Suite 102, Charlotte, NC 28208, USA). The hydrophobicity of differing fiber scaffolds was determined as follows: 10 μL of DIW was placed on top of each scaffold design. Three temporal images were taken on intervals of 1 s. Computational analysis was used to calculate the contact angle of the obtained images. Test procedures were performed in triplicate per fiber scaffold (n = 3).

Author Manuscript Author Manuscript Author Manuscript Author Manuscript

Cell Culture.

Primary human umbilical artery smooth muscle cells (HUASMCs) were cultured in a smooth muscle cell growth medium (PromoCell GmbH, Heidelberg, Germany) supplemented with 1% (v/v) antibiotic–antimycotic (Life Technologies, Carlsbad, CA, USA), 5% (v/v) fetal bovine serum (Life Technologies, Carlsbad, CA, USA), 0.5 ng/mL epidermal growth factor (EGF), 2 ng/mL basic fibroblast growth factor (bFGF), and 5 μg/mL insulin. All cells were incubated at 37 °C and 5% CO_2 and grown to 70% confluency before use in experiments. Cells between passages 3 and 6 were employed for adhesion studies.

Cell Adhesion and Retention.

Prior to cell experiments, scaffolds were dry-incubated at 55 °C for 3 h followed by 15 min UV light exposure for sterilization. Scaffolds were cut into squares (1 × 1 cm) and presoaked in media for 10 min before cell seeding. HUASMCs (25,000 cells/mL) were added to each scaffold and incubated in a humidified incubator at 37 °C and 5% CO_2 for 24 h. After 24 h, seeded scaffolds were washed in phosphate-buffered saline (PBS) × 3 to remove nonadherent cells. Scaffolds were then fixed in 4% (v/v in PBS) paraformaldehyde solution followed by blocking buffer rinse (3% BSA v/v in PBS) and permeabilization (0.5% Triton v/v in PBS). Fluoroshield with DAPI (20 μL) was added to each scaffold, which was then mounted on a microscope slide for imaging. Each scaffold was viewed and studied in five random regions, and three images were captured per region at 10× using an inverted fluorescence microscope (Axiovert 135, Carl Zeiss Microscopy LLC). Cell/microscope fields were determined from resultant images using ImageJ using a cell counter plug-in.

Statistical Analysis.

All experiments were performed in triplicate, at a minimum. A two-tailed Welch's t test was used to compare between means of each scaffold characterization, with a p value < 0.05 indicating significant differences. Correlation analysis between cell adhesion and scaffold parameters was performed using Pearson's correlation coefficient (R^2).

RESULTS

Physical Characterization of Patterned Scaffolds.

For the patterned collector designs tested, all were successfully transposed and etched onto a copper-clad circuit board laminate as targets (Figure 2a). Similarly, all trace designs generated were successful in serving as conductive targets, all accumulating PLGA fibers upon polymer jetting via electro-spinning (Figure 2b). At the macroscopic level, each unique design was effective in generating a corresponding, distinguishable, and electrospun polymer construct (Figure 2b). Despite design complexity differences and a range of target copper trace areas, i.e., ranging from 223.2 mm^2 (74% of the target exposed) to 132.3 mm^2 (44% of the target exposed), PLGA fibers remained largely confined to the traces, with the nonconductive intertrace areas remaining polymer-free.

Author Manuscript Author Manuscript Author Manuscript Author Manuscript

As to individual fiber dimensions, despite differences in copper trace patterns, the fiber diameter generated during electrospinning remained within a narrow range, varying from 4.1 to 3.4 μm, with a decline to 3.2 μm for a solid collector (Table 1). The differences observed in the fiber diameter for each trace pattern were statistically significant. The mean fiber diameter for all designs tested was 3.6 μm.

Noticeably, differing patterns of collector trace designs differed in their degree of coverage by electrospun fibers. An inverse relationship was revealed between fiber excess and the degree of total target area exposed as usable copper target traces, i.e., the copper trace area (%). As the exposed copper trace area increased from 44.1 to 74.4%, fiber excess decreased from 85.5 ± 7.6 to 52.2 ± 11.9 mm^2 ($p < 0.05$). Similarly, normalized fiber excess decreased from 64.6 to 23.4%. Having less exposed copper trace per overall target area (300 mm^2) resulted in more generous coverage of traces, resulting in more robust deposition of fibers on traces, with an apparent spillover of polymer bundles beyond trace boundary edges (e.g., see Figure 2a,b for lines and sinusoid designs).

Differing target designs also impacted the area density or fiber grammage of fibers deposited, ranging from 24.9 $\mu g/mm^2$ for the line target pattern to 17.2 $\mu g/mm^2$ for a solid target (Table 1). Relatedly, fiber excess, with polymer bundle spillover, was also linearly related to fiber grammage. Fiber grammage was found to be directly related to fiber excess, ranging from 24.9 $\mu g/mm^2$ with a normalized excess of 64.6% (line design) to 17.6 $\mu g/mm^2$ with a normalized excess of 23.4% (zigzag design) (Table 1). Similar to fiber excess, fiber grammage was noted to be inversely related to the copper trace area. As the exposed target copper trace area decreased, the grammage or packing density of the fibers increased for a given design. Statistically significant differences in fiber grammage were found between line and zigzag target designs ($p < 0.05$) as well as between line and solid designs ($p < 0.05$).

Mechanical Characterization of Patterned Scaffolds.

To define the bulk mechanical properties of the patterned scaffolds, dynamic mechanical analysis was performed on each design (3 × 1 cm). Figure 3a reveals the stress–strain relationship with uniaxial tensile testing of each PLGA scaffold design. Spin-coated PLGA was also measured as a comparative control (Figure 3b). The Young's modulus and tensile yield point of each scaffold design are listed in Table 2. Electrospun scaffold stiffness ranged from 0.3 ± 0.2 MPa (line and sinusoid designs) to 0.6 ± 0.4 MPa (solid design). As to tensile strength, the average yield point between scaffolds trended similarly to that of the Young's modulus, ranging between 0.4 ± 0.4 MPa (lines) and 0.9 ± 0.8 MPa (solid), though no statistical difference was noted for these parameters for the scaffold designs tested. Notably, the spin-coated scaffold had significantly higher stiffness and yield stress than all electrospun scaffolds tested, exhibiting approximately a 10-fold increase in stiffness (Young's modulus = 9.7 ± 2.3 MPa) and a 15-fold greater yield point (15.1 ± 2.5 MPa).

Chemical Characterization of Scaffolds.

FTIR was performed on all electrospun target designs. Spectra are shown in Figure 4. No differences were detected between the spectra generated from PLGA fiber scaffold designs

Author Manuscript Author Manuscript Author Manuscript Author Manuscript

tested. Similarly, no difference in spectra was noted between basal preprocessed PLGA and any of the post-spun PLGA derived from the various scaffold designs.

Wettability of the fiber scaffolds generated via differing targets was also assessed via measurement of the contact angle (Figure 5). The contact angle ranged from 98° with the line design to 134° for the solid target design, a change of 36% relative to the line design. The contact angle was noted to vary inversely with fiber excess and with fiber grammage.

Cell Adhesion and Retention of Scaffolds.

The impact of electrospun scaffold design on cell adhesion and retention at 24 h was determined via measurement of the number of vascular smooth muscle cells (VSMCs) per microscope field detected in random regions of each construct postincubation and washing. Of all scaffold designs tested, the line design exhibited the highest adhesion and retention followed by sinusoids and squares, which were all significantly greater than the solid electrospun sample ($p < 0.01$; Figure 6a.) Cell counts ranged from 257.9 VSMC/field for the line design to 149.8 VSMC/field for the solid target at 24 h, a decrease of 42% relative to the line design. Cell adhesion was significantly lower with the spin-coated PLGA than all electrospun scaffolds tested ($p < 0.01$).

As to the influence of bulk scaffold construct properties on cell adhesion and retention, there was an inverse relationship between cell adhesion and fiber target coverage (%). As overall target surface area coverage increased from 72.6% with the line design to 100% for the solid design, cell adhesion and retention decreased from 257.9 VSMC/field for the line design to 149.8 VSMC/field at 24 h ($R^2 = 0.94$; Figure 6b).

As to macroporosity, there was a direct correlation between cell adhesion and retention at 24 h and scaffold residual open area (%). Cell adhesion varied from 95.8 VSMC/field for the solid design to 257.9 VSMC/field for the line design ($R^2 = 0.94$; Figure 6c).

As to the impact of bulk fiber density, there was a direct correlation between cell adhesion and retention at 24 h and normalized fiber excess ($R^2 = 0.99$; Figure 6d). At 0% fiber excess, as exists in the continuous solid target design, a baseline cell adhesion of 149.8 VSMC/field was detected. As fiber excess increased to a maximum of 64.6% for the line design, cell adhesion and retention increased to 257.9 VSMC/field, an increase of 172% relative to the solid design. Similarly, this construct density to cell adhesion and retention relationship was also noted for fiber grammage ($R^2 = 0.72$; Figure 6e). As bulk construct density increased from a minimum of 17.2 $\mu g/mm^2$ with the solid construct to a maximum of 24.9 $\mu g/mm^2$ for the line design, cell adhesion increased correspondingly.

DISCUSSION

Tailoring fibrous constructs to create specific indication matrices, recapitulating individual organ or tissue nuances for specific therapeutic indications, is an overall goal of tissue engineering. Electrospinning by virtue of its ability to generate fine fibers from a range of natural and synthetic biomaterials has always been looked upon with promise for this purpose, though it has been limited to date in its broad ability to generate constructs of

Author Manuscript Author Manuscript Author Manuscript Author Manuscript

defined overall design, fiber bundle morphology, and fiber density. Here, we examined the efficacy of employing designated pattern electrospinning conductive targets, with specific exposed electroconductive trace patterns, as a means of generating defined, reproducible fiber constructs with a range of complexity. We demonstrate that the definition of such targets indeed enabled control of subsequent electrospun fiber deposition, construct bulk configuration, and scaffold macroscopic properties. Nevertheless, differing constructs had identical chemical compositions and similar bulk mechanical properties. The impact of differing pattern constructs was revealed in that each had distinct physical characteristics, which influenced cell adhesion and retention. Specifically, macroscopic spacing between bulk fiber bundles, fiber bundle density, and construct surface tension all influenced cell adhesion, retention, and growth at 24 h. Overall, our results indicate the ability to tune a macroscale fiber construct scaffold design, via manipulation of electro-spinning target patterns, which ultimately influences microscale cell–material interactions.

Efficacy of Patterned Targets as Fiber Collectors and Construct Formers.

In the present study, we demonstrated that custom designing a flat electrospinning target to create macroscopic constructs of fibers is a viable method. For all designs examined, effective deposition of fibers was reproducibly detected, suggesting its efficacy as a viable processing methodology for creating complex, shape-dictated constructs. Over a range of exposed traces ranging from 72.6 to 100% conductive surface, in no case did gapping or uneven distribution of fibers occur macroscopically or microscopically in terms of density, i.e., grammage. This approach offers utility in the formation of single-target constructs or in layering to create multilayer targets, which may be applied one on top of another to create increasing thickness. What remains unknown are the limits of copper trace geometry influence on single fiber and fiber construct parameters.

Prior published works have largely examined the manipulation of conductive targets for successful control of individual fiber alignment[39–41] and fabrication of single-fiber latticework or constructs with three-dimensional characteristics.[42,43] The present study extends fabrication investigation beyond these areas to the ability to control deposition of randomly oriented fibers in larger bundle constructs via manipulation of exposed copper trace dimensions and configurations. As to the macrodeposition of fiber bundles, our results revealed interesting behavior based on the target pattern. It became clear that as the total percent conductive target decreased, open nonconductive areas increased, and macroscopic fiber bundles generated on a given trace increased in terms of fiber excess, extending beyond the trace boundary. Pan et al. similarly found that decreasing the conductive area exposed to electrospinning qualitatively led to higher deposition on nonconductive portions of the collector.[39] We also found that a related inverse relationship existed in terms of fiber density, with denser fiber bundles being deposited on more sparse targets, i.e., with a lower % exposed copper trace area. This finding also agreed with prior work of others demonstrating higher electrospun fiber density in areas adjacent to conductive target zones associated with non-conductive gaps and areas exposed.[44]

The variation in the copper trace pattern in relation to fiber parameters, i.e., fiber deposition density on copper traces and open residual area, in particular, is influenced by the imposed

Author Manuscript Author Manuscript Author Manuscript Author Manuscript

electric field. A main driver of fiber deposition is the magnitude and direction of the electrical field generated between the syringe needle and the target.[45,46] Our electrospun scaffolds were all constructed by utilizing the same electric field magnitude. Therefore, any influence of the electric field on fiber construct properties was likely due to varying directions or trajectories of the electric field. Specifically, in the line pattern, the electric field forms clear and distinct organized field lines and vectors between the jet nozzle and the grounded collector, with small variations near the collector. In contrast, electrospinning with the denser and geometrically complex zigzag design target increased distortion of the electric field, and fringe effects near the edges of the zigzag pattern of the collector occurred, influencing polymer jet trajectory and resulting in less overall deposition over the copper trace patterns. The influence of the electric field on electrospun fiber formation has been previously examined. Utilizing a range of nonconductive meshes to alter electric field configuration and intensity, Zhao et al. demonstrated that manipulations that disturb the electric field, lowering the electrostatic interaction between the electrospinning jet and the collector, resulted in reduced fiber deposition.[41] Similarly, Secasanu et al. demonstrated that the alignment of the electric field was directly correlated with the robustness of fiber deposition.[47]

As to individual fiber morphology, work by others has shown that the fiber diameter has been noted to change with polymer concentration and applied voltage.[48,49] These variables all remained constant in this study. SEM of all fiber constructs generated here all revealed similar morphology at the level of resolution achievable by electron microscopic imaging. All target shapes tested led to fiber diameters differing over a very narrow range. This tight range of fiber diameters was consistent with prior published data on the use of a uniform electrospinning protocol, as was employed in this study.

Effect of Target Design on Mechanical and Chemical Properties of Constructs.

All fiber constructs generated utilized identical electrospinning conditions, i.e., polymer concentration, solvent, molecular weight, applied voltage, and distance to the target. Despite generating a range of shapes with differing fiber grammage, no difference in chemical composition was noted. These results are consistent with observations of others that similarly reported unaltered chemical composition despite a range of polymer fabrication processes.[50,51] What differed between scaffold designs were surface free energy and overall hydrophobicity. In general, the greater the bulk net polymer deposition per scaffold design tested, the greater was the hydrophobicity observed.

No significant difference in mechanical properties was noted between designs tested. While a trend to greater stiffness was seen for denser constructs, i.e., with a solid sheet being greater than all other designs, all shapes generated were of the same order of magnitude as bulk material properties. This finding is noteworthy in that it demonstrates that one may alter cellular adhesivity over a range, as shown in Figure 6, while maintaining similar mechanical properties.

Author Manuscript Author Manuscript Author Manuscript Author Manuscript

Construct Macroscopic Openness, Fiber Bundle Configuration, and Fiber Grammage Influence Cell Behavior.

A clear relationship was observed between construct macroscopic configuration properties and cell adhesion and retention. As macroscopic “openness” of designs increased from 0% in the solid configuration to 27.4% in the line configuration, cell adhesion and retention increased. Interestingly, this data on macroscopic “openness” supports the concept that cells favor a more porous design polymer construct for in-migration, attachment, survival, and growth. Consistent with our observation is the work by Vaquette and Cooper-White who reported a greater degree of fibroblast penetration into scaffolds specifically fabricated with larger macroporosity compared with those of a conventional tighter design, with fiber diameters all remaining in the same narrow range.[44] Balguid et al. similarly demonstrated that construct density and porosity influenced venous myofibroblast penetration, with more porous constructs affording greater inmigration.[18] In this case, as opposed to our work, a porosity change was achieved via manipulation of fiber diameters, with the most porous in-growth favoring scaffolds formed with a maximum fiber diameter of 12.1 μm.

Beyond in-migration, cell adhesion and retention were studied here as an index of construct functional efficacy. Ultimately, the goal of use of the types of constructs generated here will be for tissue fabrication, augmentation, and repair. As such, once cells in-migrate, they require an adequate construct “substratum” for adhesion. From this perspective, our study revealed two interesting properties. A direct relationship was observed between the number of cells retained and fiber density i.e., fiber grammage. As cells functionally migrate within the bulk construct having an adequate substratum, adhesion surfaces and points of attachment are needed. Creating a denser, yet open, i.e., spun, construct provides a more effective distribution of underlying surface area for points of attachment. This is consistent with many studies in cell biology demonstrating the need for adequate contact for cell retention and survival, particularly on artificial surfaces.[52,53]

A second property revealed by this study is the utility of varying fiber excess as a determinative property for cell adhesion and retention. We demonstrate that cell adhesion and retention directly correlate with the degree of fiber excess (Figure 6d). This finding supports the concept that providing greater bulk of a favorable fibrous substratum—as discussed above—is effective as a means of increasing net cell adhesion and retention. Yet, our data suggests that limits may exist, in that as fiber excess increases to the point of actually “overcrowding” the macroconstruct configuration, decreasing residual open area, cell adhesion and retention may ultimately plateau and potentially decrease. This concept is supported by our observation of the inverse relationship observed between cell adhesion and retention and % open surface area observed (Figure 6c) This property also may relate to the relative increase in overall hydrophobicity that occurs with a net increase in the excess fiber absolute content, creating a less favorable environment. This is supported by our contact angle data demonstrating an increase in the contact angle (Figure 5) with constructs having increased % fiber target coverage (Table 1). This relationship is supported by observations of others. For example, Ayala et al. demonstrated that increased substrate hydrophobicity via an admixture of varying carbon length acryloyl amino acid monomers altered cell adhesion, finding an optimum surface and contact angle, with lower or greater contact angles, i.e.,

Author Manuscript Author Manuscript Author Manuscript Author Manuscript

lower or greater hydrophobicity, being less effective in adhesion.[54] Dowling et al. as well demonstrated that in modifying the hydrophobicity of polystyrene, cell adhesion would vary, with optimal adhesion of osteoblasts observed at 108–110°, with adhesion falling off with angles of 125–155°.[55] Our contact angle optimum here was 100°, consistent with the observation of optimal cell behavior reported.

Study Limitations.

The fibrous nature of our constructs made it difficult to utilize certain analytical methods for direct measurements of local properties. Specifically, atomic force microscopy (AFM) valuable for providing vital information regarding regional stiffness and quantifiable topographic features was problematic. We found that PLGA fibers were difficult to probe with AFM without significantly damaging the scaffold or the probe itself. Future studies will examine other methods to further investigate fiber construct properties, beyond those reported here, to further define the connection between construct properties and cell behavior. Additionally, in this work, we investigated the interaction of one cell type with the scaffold constructs. Future studies will examine the behavior of other cells, of differing embryonic origin, to determine the generality of our observations. Finally, the ability to extend construct fabrication using this method to multi-layered constructs remains to be defined.

CONCLUSIONS

Alteration of conductive electrospinning trace patterns appears to be an effective means of directing and manipulating the macroscopic fabrication of electrospun fiber constructs. While utilizing similar electrical jetting parameters and a common polymeric solution, a range of fiber target coverage may be achieved despite having an underlying common overall target area. Varying the trace conductive area and spacing is an effective means of altering macroscopic fiber deposition, effectively modifying macroporosity. Interestingly, trace spacing, via electrical field manipulation, alters fiber deposition density. All of these manipulations, while not impacting chemical and mechanical properties of constructs, directly alter cell adhesion and retention with greater macroporosity, fiber excess, and fiber grammage directly impacting cell adhesion and retention, demonstrating their value as manipulable variables for construct fabrication for varying tissue engineering purposes.

ACKNOWLEDGMENTS

The authors acknowledge the Arizona Center for Accelerated Biomedical Innovation (ACABI) for funding support and the NIH Cardiovascular Biomedical Engineering Training Grant (T32 HL007955).

REFERENCES

(1). Roy V; Magne B; Vaillancourt-Audet M; Blais M; Chabaud S; Grammond E; Piquet L; Fradette J; Laverdière I; Moulin VJ; Landreville S; Germain L; Auger F; Gros-Louis F; Bolduc S Human Organ-Specific 3D Cancer Models Produced By The Stromal Self-Assembly Method Of Tissue Engineering For The Study Of Solid Tumors. BioMed Res. Int 2020, 2020, 1–23.

(2). Sreekala P; Suresh M; Lakshmi Priyadarsini S 3D Organ Printing: Review On Operational Challenges And Constraints. Mater. Today: Proc 2020, 4703.

Author Manuscript Author Manuscript Author Manuscript Author Manuscript

(3). Tang SW; Tong WY; Pang SW; Voelcker NH; Lam YW Deconstructing, Replicating, And Engineering Tissue Micro-environment For Stem Cell Differentiation. Tissue Eng., Part B 2020, 540.

(4). Honig F; Vermeulen S; Zadpoor AA; De Boer J; Fratila-Apachitei LE Natural Architectures For Tissue Engineering And Regenerative Medicine. J. Funct. Biomater 2020, 11, 47.

(5). Lowen JM; Leach JK Functionally Graded Biomaterials For Use As Model Systems And Replacement Tissues. Adv. Funct. Mater 2020, 30, 1909089. [PubMed: 33456431]

(6). Fitzpatrick LE; McDevitt TC Cell-Derived Matrices For Tissue Engineering And Regenerative Medicine Applications. Biomater. Sci 2015, 3, 12–24. [PubMed: 25530850]

(7). Rana D; Zreiqat H; Benkirane-Jessel N; Ramakrishna S; Ramalingam M Development Of Decellularized Scaffolds For Stem Cell-Driven Tissue Engineering. J. Tissue Eng. Regener. Med 2015, 11, 942–965.

(8). Chung HJ; Park TG Injectable Cellular Aggregates Prepared From Biodegradable Porous Microspheres For Adipose Tissue Engineering. Tissue Eng., Part A 2009, 15, 1391–1400. [PubMed: 19327016]

(9). D'Amore A; Yoshizumi T; Luketich SK; Wolf MT; Gu X; Cammarata M; Hoff R; Badylak SF; Wagner WR Bi-Layered Polyurethane – Extracellular Matrix Cardiac Patch Improves Ischemic Ventricular Wall Remodeling In A Rat Model. Biomaterials 2016, 107, 1–14. [PubMed: 27579776]

(10). Leong KF; Cheah CM; Chua CK Solid Freeform Fabrication Of Three-Dimensional Scaffolds For Engineering Replacement Tissues And Organs. Biomaterials 2003, 24, 2363–2378. [PubMed: 12699674]

(11). Rajab TK; O'Malley TJ; Tchantchaleishvili V Decellularized Scaffolds For Tissue Engineering: Current Status And Future Perspective. Artif. Organs 2020, 44, 1031–1043. [PubMed: 32279344]

(12). Huang ZM; Zhang YZ; Kotaki M; Ramakrishna S A Review On Polymer Nanofibers By Electrospinning And Their Applications In Nanocomposites. Compos. Sci. Technol 2003, 63, 2223–2253.

(13). Teo WE; Inai R; Ramakrishna S Technological Advances In Electrospinning Of Nanofibers. Sci. Technol. Adv. Mater 2011, 12, No. 013002. [PubMed: 27877375]

(14). Cai S; Xu H; Jiang Q; Yang Y Novel 3D Electrospun Scaffolds With Fibers Oriented Randomly And Evenly In Three Dimensions To Closely Mimic The Unique Architectures Of Extracellular Matrices In Soft Tissues: Fabrication And Mechanism Study. Langmuir 2013, 29, 2311–2318. [PubMed: 23390966]

(15). Kim BS; Mooney DJ Development Of Biocompatible Synthetic Extracellular Matrices For Tissue Engineering. Trends Biotechnol. 1998, 16, 224–230. [PubMed: 9621462]

(16). Teo WE; Ramakrishna S A Review On Electrospinning Design And Nanofibre Assemblies. Nanotechnology 2006, 17, R89–R106. [PubMed: 19661572]

(17). Zhang D; Chang J Patterning Of Electrospun Fibers Using Electroconductive Templates. Adv. Mater 2007, 19, 3664–3667.

(18). Balguid A; Mol A; van Marion MH; Bank RA; Bouten CV; Baaijens FP Tailoring Fiber Diameter In Electrospun Poly(ε-Caprolactone) Scaffolds For Optimal Cellular Infiltration In Cardiovascular Tissue Engineering. Tissue Eng., Part A 2009, 15, 437–444. [PubMed: 18694294]

(19). Wong SC; Baji A; Leng S Effect Of Fiber Diameter On Tensile Properties Of Electrospun Poly(ε-Caprolactone). Polymer 2008, 49, 4713–4722.

(20). Teo WE; He W; Ramakrishna S Electrospun Scaffold Tailored For Tissue-Specific Extracellular Matrix. Biotechnol. J 2006, 1, 918–929. [PubMed: 16941439]

(21). Merkle VM; Zeng L; Slepian MJ; Wu X Core-Shell Nanofibers: Integrating The Bioactivity Of Gelatin And The Mechanical Property Of Polyvinyl Alcohol. Biopolymers 2014, 101, 336–346. [PubMed: 23913748]

(22). Merkle VM; Tran PL; Hutchinson M; Ammann KR; DeCook K; Wu X; Slepian MJ Core–Shell PVA/Gelatin Electrospun Nanofibers Promote Human Umbilical Vein Endothelial Cell And Smooth Muscle Cell Proliferation And Migration. Acta Biomater. 2015, 27, 77–87. [PubMed: 26320540]

Author Manuscript Author Manuscript Author Manuscript Author Manuscript

(23). Merkle VM; Martin D; Hutchinson M; Tran PL; Behrens A; Hossainy S; Sheriff J; Bluestein D; Wu X; Slepian MJ Hemocompatibility Of Poly(Vinyl Alcohol)–Gelatin Core–Shell Electrospun Nanofibers: A Scaffold For Modulating Platelet Deposition And Activation. ACS Appl. Mater. Interfaces 2015, 7, 8302–8312. [PubMed: 25815434]

(24). Liu C; Zhu C; Li J; Zhou P; Chen M; Yang H; Li B The Effect Of The Fibre Orientation Of Electrospun Scaffolds On The Matrix Production Of Rabbit Annulus Fibrosus-Derived Stem Cells. Bone Res. 2015, 3, 15012. [PubMed: 26273539]

(25). Soliman S; Sant S; Nichol JW; Khabiry M; Traversa E; Khademhosseini A Controlling The Porosity Of Fibrous Scaffolds By Modulating The Fiber Diameter And Packing Density. J. Biomed. Mater. Res., Part A 2011, 96A, 566–574.

(26). Sundararaghavan HG; Metter RB; Burdick JA Electrospun Fibrous Scaffolds With Multiscale And Photopatterned Porosity. Macromol. Biosci 2009, 10, 265–270.

(27). Ifkovits JL; Sundararaghavan HG; Burdick JA Electrospinning Fibrous Polymer Scaffolds For Tissue Engineering And Cell Culture. J. Visualized Exp 2009, 32, No. e1590.

(28). Wu J; Hong Y Enhancing Cell Infiltration Of Electrospun Fibrous Scaffolds In Tissue Regeneration. Bioact. Mater 2016, 1, 56–64. [PubMed: 29744395]

(29). Han DG; Ahn CB; Lee JH; Hwang Y; Kim JH; Park KY; Lee JW; Son KH Optimization Of Electrospun Poly(Caprolactone) Fiber Diameter For Vascular Scaffolds To Maximize Smooth Muscle Cell Infiltration And Phenotype Modulation. Polymer 2019, 11, 643.

(30). Tan GZ; Zhou Y Tunable 3D Nanofiber Architecture Of Polycaprolactone By Divergence Electrospinning For Potential Tissue Engineering Applications. Nano-Micro Lett. 2018, 10, 1–10.

(31). Abed Al-Hazeem N Nanofibers And Electrospinning Method; 2017. DOI: 10.5772/intechopen.72060

(32). Karakaş H Electrospinning of nanofibers and their applications; Istanbul Technical University: Textile Technologies and Design Faculty, 2015.

(33). Bhardwaj N; Kundu SC Electrospinning: A Fascinating Fiber Fabrication Technique. Biotechnol. Adv 2010, 28, 325–347. [PubMed: 20100560]

(34). Kurečič M; Smole MS Electrospinning: Nanofibre Production Method Tekstilec 56, no. 1 2013.

(35). Nurwaha D; Han W; Wang X Investigation Of A New Needleless Electrospinning Method For The Production Of Nanofibers. J. Eng. Fibers Fabr 2013, 8, 155892501300800.

(36). Naghizadeh F; Solouk A; Khoulenjani SB Osteochondral Scaffolds Based On Electrospinning Method: General Review On New And Emerging Approaches. Int. J. Polym. Mater. Polym. Biomater 2017, 67, 913–924.

(37). Baji A; Mai YW; Wong SC; Abtahi M; Chen P Electrospinning Of Polymer Nanofibers: Effects On Oriented Morphology, Structures And Tensile Properties. Compos. Sci. Technol 2010, 70, 703–718.

(38). Nemati S; Kim SJ; Shin YM; Shin H Current Progress In Application Of Polymeric Nanofibers To Tissue Engineering. Nano Convergence 2019, 6, 36. [PubMed: 31701255]

(39). Pan C; Han YH; Dong L; Wang J; Gu ZZ Electrospinning Of Continuous, Large Area, Latticework Fiber Onto Two-Dimensional Pin-Array Collectors. J. Macromol. Sci., Part B: Phys 2008, 47, 735–742.

(40). Gibson P; Schreuder-Gibson H Patterned Electrospray Fiber Structures. Int. Nonwovens J 2004, 1558925004os–1551300211os.

(41). Zhao S; Zhou Q; Long YZ; Sun GH; Zhang Y Nanofibrous Patterns By Direct Electrospinning Of Nanofibers Onto Topographically Structured Non-Conductive Substrates. Nanoscale 2013, 5, 4993. [PubMed: 23636504]

(42). Holjevać Grguric T; Mijović B; Zdraveva E; Govorčin Bajsić E; Slivac I; Ujčić M; Dekaris I; Tominac Trcin M; Vuković A; Kuzmić S; et al. Electrospinning Of PCL/CEFUROXIM® Fibrous Scaffolds On 3D Printed Collectors. J. Text. Inst 2020, 111, 1288–1299.

(43). Zhang D; Chang J Electrospinning Of Three-Dimensional Nanofibrous Tubes With Controllable Architectures. Nano Lett. 2008, 8, 3283–3287. [PubMed: 18767890]

(44). Vaquette C; Cooper-White JJ Increasing Electrospun Scaffold Pore Size With Tailored Collectors For Improved Cell Penetration. Acta Biomater. 2011, 7, 2544–2557. [PubMed: 21371575]

Author Manuscript Author Manuscript Author Manuscript Author Manuscript

(45). Angammana CJ; Jayaram SH Investigation Of The Optimum Electric Field For A Stable Electrospinning Process. IEEE Trans. Ind. Appl 2012, 48, 808–815.

(46). Kong CS; Lee TH; Lee SH; Kim HS Nano-Web Formation By The Electrospinning At Various Electric Fields. J. Mater. Sci 2007, 42, 8106–8112.

(47). Secasanu VP; Giardina CK; Wang Y A Novel Electrospinning Target To Improve The Yield Of Uniaxially Aligned Fibers. Biotechnol. Prog 2009, 25, 1169–1175. [PubMed: 19562742]

(48). Mo XM; Xu CY; Kotaki MEA; Ramakrishna S Electrospun P(LLA-CL) Nanofiber: A Biomimetic Extracellular Matrix For Smooth Muscle Cell And Endothelial Cell Proliferation. Biomaterials 2004, 25, 1883–1890. [PubMed: 14738852]

(49). Yang Y; Jia Z; Liu J; Li Q; Hou L; Wang L; Guan Z Effect Of Electric Field Distribution Uniformity On Electrospinning. J. Appl. Phys 2008, 103, 104307.

(50). Khalil KA; Fouad H; Elsarnagawy T; Almajhdi FN Preparation And Characterization Of Electrospun PLGA/Silver Composite Nanofibers For Biomedical Applications. Int. J. Electrochem. Sci 2013, 8, 3483–2493.

(51). Esmaili Z; Bayrami S; Dorkoosh FA; Akbari Javar H; Seyedjafari E; Zargarian SS; Haddadi-Asl V Development And Characterization Of Electrosprayed Nanoparticles For Encapsulation Of Curcumin. J. Biomed. Mater. Res., Part A 2017, 106, 285–292.

(52). Massia SP; Hubbell JA An RGD Spacing Of 440 Nm Is Sufficient For Integrin Alpha V Beta 3-Mediated Fibroblast Spreading And 140 Nm For Focal Contact And Stress Fiber Formation. J. Cell Biol 1991, 114, 1089–1100. [PubMed: 1714913]

(53). Chen CS; Mrksich M; Huang S; Whitesides GM; Ingber DE Geometric Control Of Cell Life And Death. Science 1997, 276, 1425–1428. [PubMed: 9162012]

(54). Ayala R; Zhang C; Yang D; Hwang Y; Aung A; Shroff SS; Arce FT; Lal R; Arya G; Varghese S Engineering The Cell–Material Interface For Controlling Stem Cell Adhesion, Migration, And Differentiation. Biomaterials 2011, 32, 3700–3711. [PubMed: 21396708]

(55). Dowling DP; Miller IS; Ardhaoui M; Gallagher WM Effect Of Surface Wettability And Topography On The Adhesion Of Osteosarcoma Cells On Plasma-Modified Polystyrene. J. Biomater. Appl 2010, 26, 327–347. [PubMed: 20566655]

Author Manuscript Author Manuscript Author Manuscript Author Manuscript

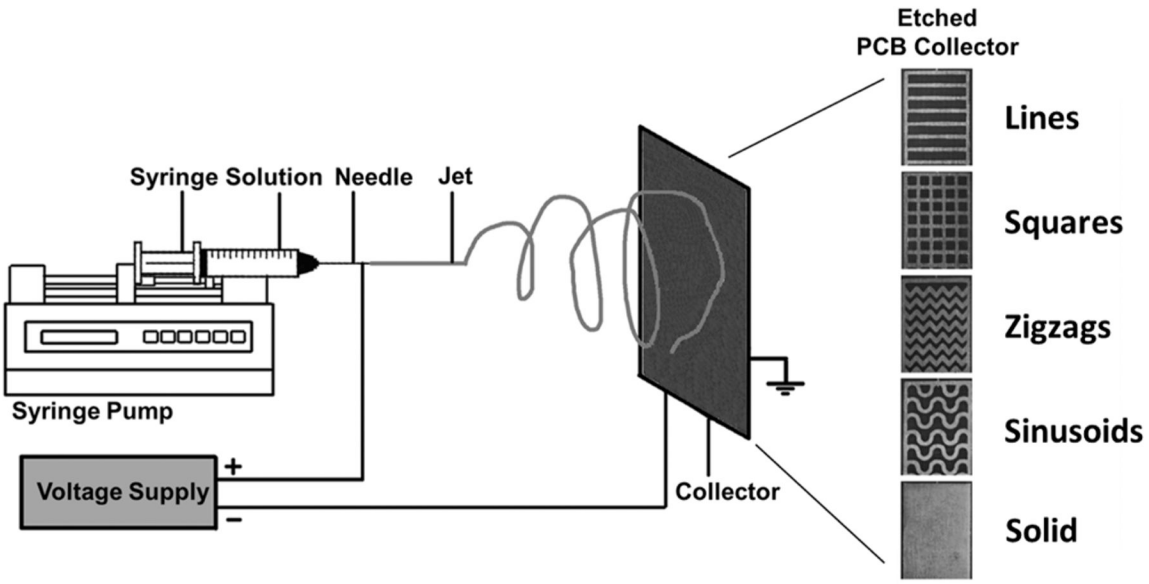

Figure 1.

Electrospinning system. The system consisted of a flow-controlled syringe pump, polymer (PLGA) solution, a high voltage supply, and a grounded collector. The grounded collectors were acid-etched to create differing fiber designs.

Author Manuscript Author Manuscript Author Manuscript Author Manuscript

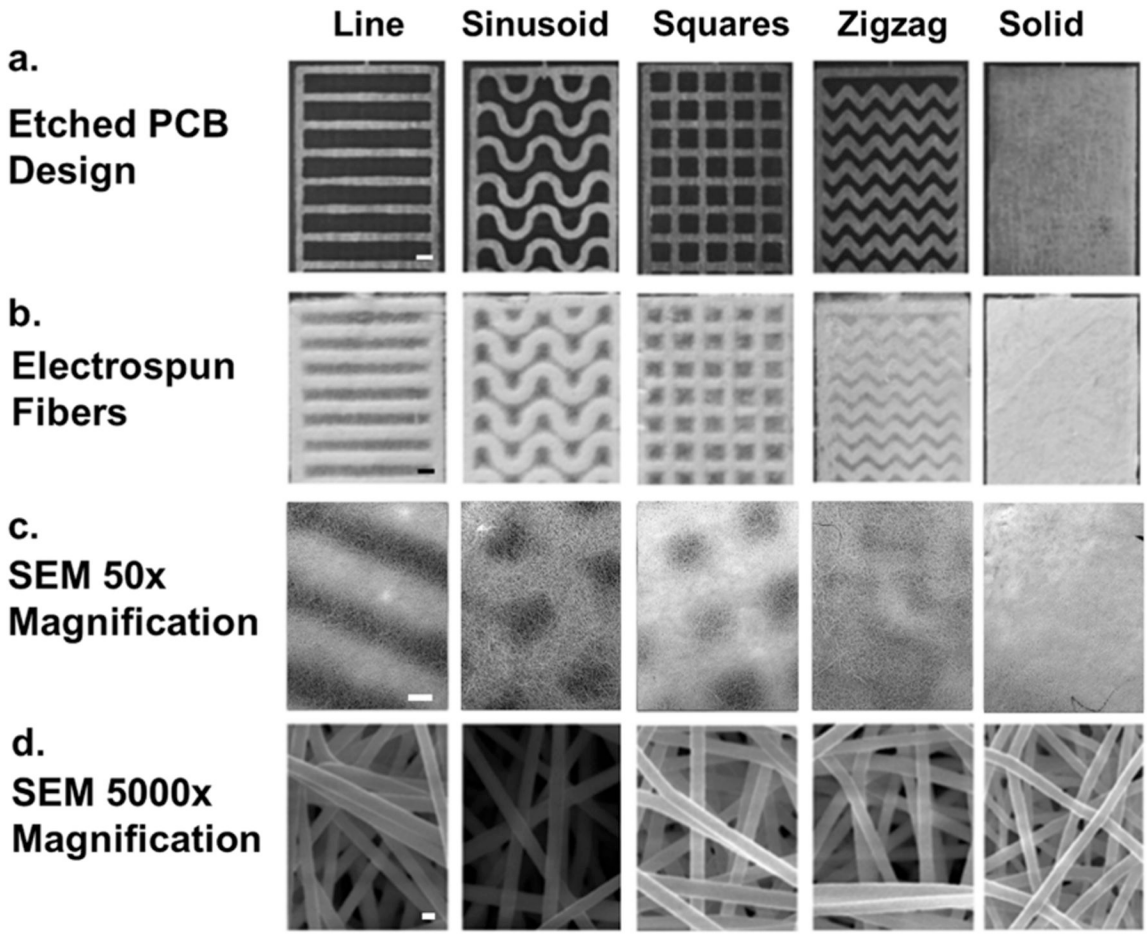

Figure 2.

Collector designs and resultant electrospun PLGA fibers. (a) Five unique conductive collector designs etched on a printed circuit board (scale bars represent 1 mm). (b) PLGA fiber patterns electrospun onto corresponding collector designs (scale bars represent 1 mm). (c) Low-powered 50× SEM images of PLGA-patterned fibers (scale bars represent 50 μm). (d) High-powered 5000× SEM images of PLGA fiber constructs on the conductive portion of the collector (scale bars represent 4 μm).

Author Manuscript Author Manuscript Author Manuscript Author Manuscript

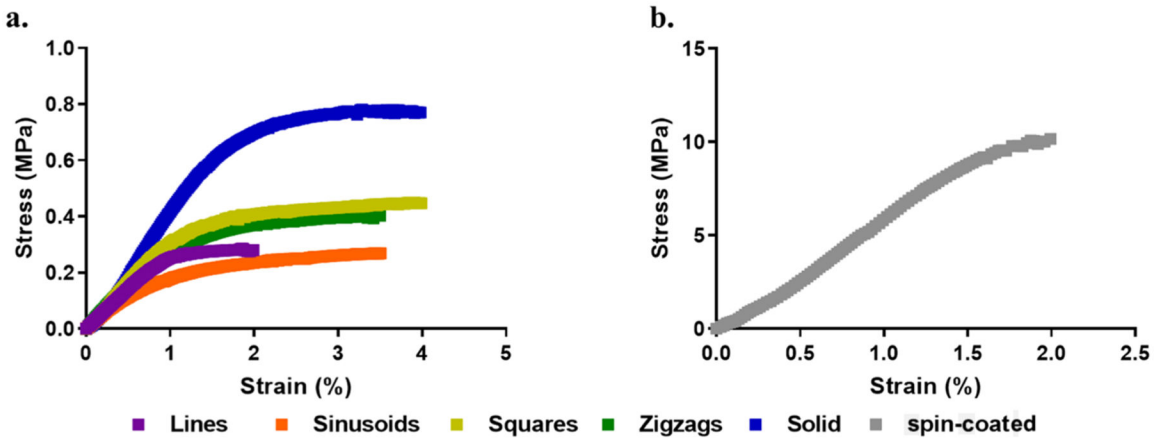

Figure 3.

Stress vs strain of the PLGA fibers and film. (a) Stress vs strain curves of PLGA fibers and (b) spin-coated PLGA film. Samples were strained until failure. The graph represents data collected from a single run.

Author Manuscript Author Manuscript Author Manuscript Author Manuscript

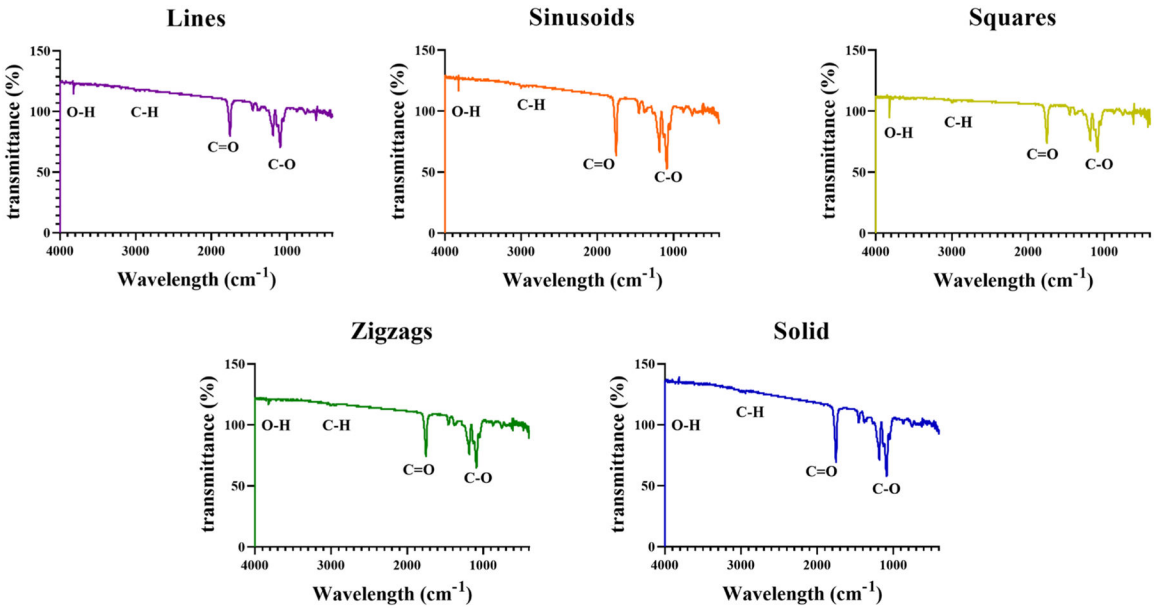

Figure 4.

FTIR of PLGA electrospun fiber scaffolds. C–O peaks between 1000 and ~1400 cm, C=O peaks between 1700 and 1800, C–H peaks between 2800 and 3100, and O–H peaks between 3700 and 3900.

Author Manuscript Author Manuscript Author Manuscript Author Manuscript

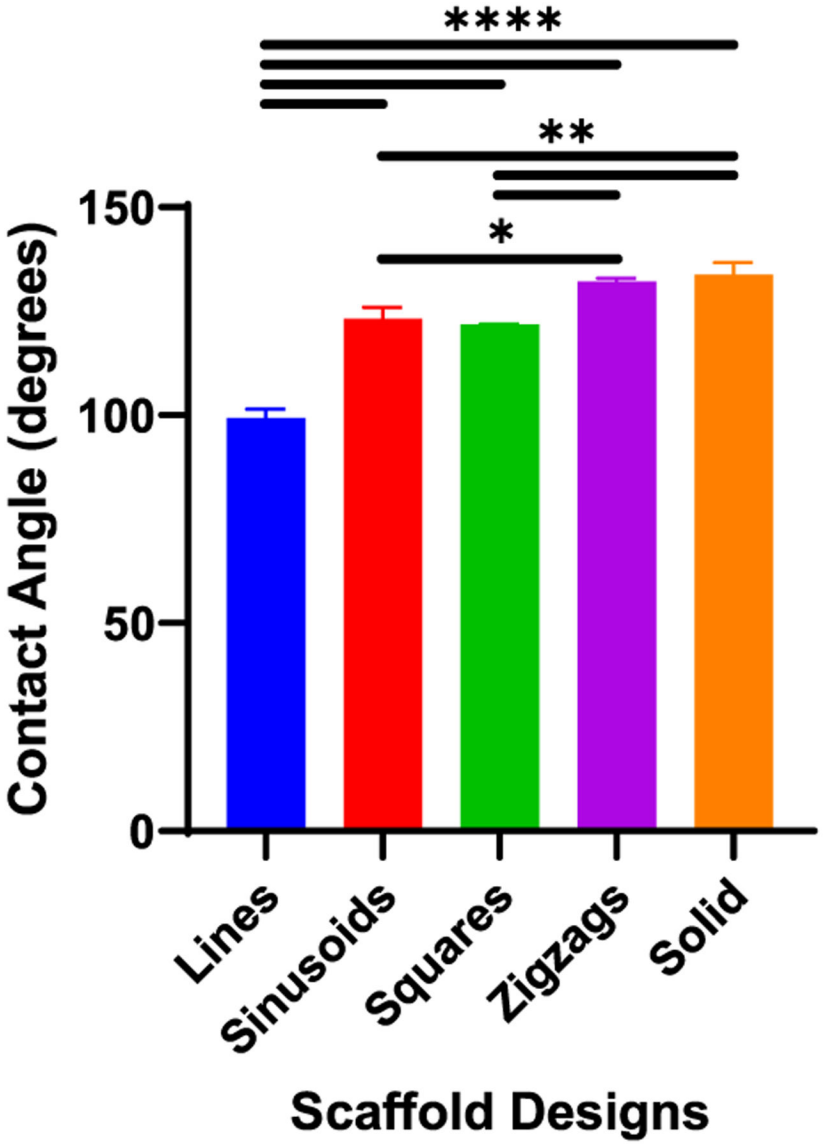

Figure 5.

Contact angle of electrospun PLGA scaffolds. The contact angle ranged from 98° (lines) to 134° (solid). An increased contact angle corresponds to greater hydrophobicity. Values are mean ± standard error ($n = 9$). * indicates $p < 0.05$; ** indicates $p < 0.01$; **** indicates $p < 0.001$.

Author Manuscript Author Manuscript Author Manuscript Author Manuscript

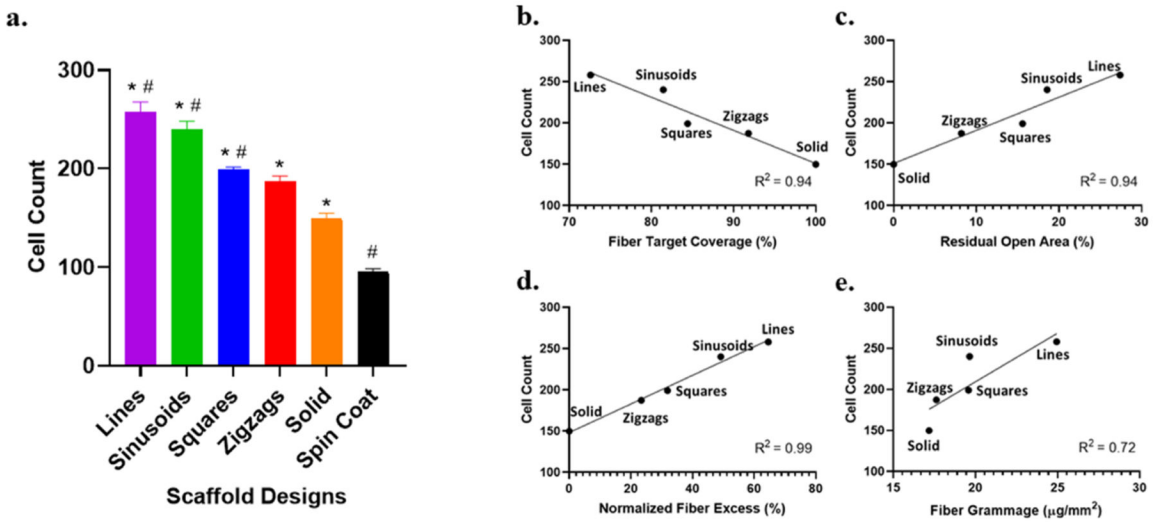

Figure 6.

Cell adhesion and retention on PLGA scaffolds after 24 h and corresponding fiber scaffold properties. (a) Vascular smooth muscle cells adherent post washing counted per 10× field by utilizing fluorescence imaging after 24 h. Values represent the mean cell count ± standard error ($n = 10$); * indicates $p < 0.05$ in reference to the spin-coated sample; # indicates $p < 0.05$ in reference to the solid PLGA fiber scaffold. (b) Cell count (per high power field 10×) as a function of fiber target coverage, (c) residual open area, (d) normalized fiber excess, and (e) fiber grammage. Values represent the mean cell count.

Author Manuscript Author Manuscript Author Manuscript Author Manuscript

Table 1.

Electrospun PLGA Fiber Construct Characteristics for Specific Collector Designs[a]

	total area (mm^2)	copper trace area (mm^2)	fiber (scaffold) area (mm^2)	fiber diameter (μm)	weight (mg)	fiber grammage $\mu g/mm^2$)	fiber excess (mm^2)	normalized copper trace area (%)	fiber target coverage (%)	normalized fiber excess (%)	residual open area (%)
lines	300	132.3	217.8 ± 7.6	4.0 ± 0.0	5.4 ± 1.4	24.9 ± 0.8	85.5 ± 7.6	44.1	72.6 ± 1.3	64.6 ± 5.8	27.4 ± 2.5
sinusoids	300	163.8	244.2 ± 12.1	3.4 ± 0.	4.8 ± 1.4	19.6 ± 0.9	80.5 ± 12.7	54.6	81.4 ± 2.1	49.2 ± 7.8	18.6 ± 4.2
squares	300	192.0	253.2 ± 19.9	3.6 ± 0.1	4.9 ± 2.1	19.6 ± 1.3	61.2 ± 19.9	64.0	84.4 ± 3.3	31.9 ± 10.3	15.6 ± 6.6
zigzags	300	223.2	275.4 ± 11.9	4.1 ± 0.0	4.8 ± 1.5	17.6 ± 0.7	52.2 ± 11.9	74.4	91.8 ± 2.0	23.4 ± 5	8.2 ± 4.0
solid	300	300	300 ± 0.0	3.2 ± 0.0	5.2 ± 1.9	17.2 ± 0.0	0.0 ± 0.0	100	100 ± 0.0	0.0 ± 0.0	0.0 ± 0.0

[a]Values are mean ± standard deviation ($n = 4$). Total area is the area (mm^2) of the collector, including both conductive and nonconductive areas. Copper trace area is the area (mm^2) of the exposed copper trace for each design. Fiber (scaffold) area is the actual fiber coverage area (mm^2) for each design. Fiber diameter is the diameter (μm) measured of the fibers from SEM images. Fiber grammage is the "area density" of the scaffold, calculated as mass per fiber (scaffold) area of the scaffold. Normalized copper trace area is the percentage of exposed copper of the total area (300 mm^2) of each collector. Fiber target coverage is the percent of total area (300 mm^2) covered by electrospun fibers. Fiber excess is the "spillover" area of the electrospun fibers, which exceeds the bounds of the copper trace. Normalized fiber excess is the amount of fiber excess in relation to the copper trace area, an index of accuracy of the fibers distributed onto the collector. Residual open area is the percent of the full target (300 mm^2) not covered by the electrospun scaffold, the inverse of fiber target coverage.

ACS Appl Bio Mater. Author manuscript; available in PMC 2022 September 05.

Author Manuscript

Author Manuscript

Author Manuscript

Author Manuscript

Table 2.

The Young's Modulus and Tensile Strength of the PLGA Fiber Constructs and Film[a]

	Young's modulus (MPa)	yield point (MPa)
lines	0.3 ± 0.2	0.4 ± 0.4
sinusoids	0.3 ± 0.2	0.4 ± 0.3
squares	0.4 ± 0.2	0.5 ± 0.4
zigzags	0.3 ± 0.2	0.5 ± 0.4
solid	0.6 ± 0.4	0.9 ± 0.8
spin coat	9.8 ± 5.6	15.1 ± 6.1

[a]Values are mean ± standard deviation ($n = 6$).